Supplementary Information (SI)

In-situ growth of conductive bimetallic catecholates MOFs on porous graphene for high-performance formaldehyde gas sensing.

Anh Tuan Trong Tran[a], Kamrul Hassan[a], M. A. Jalil[a], Tran Thanh Tung[a], Tetsuya Kida[b], and Dusan Losic[a*]

[a] School of Chemical Engineering, The University of Adelaide, Adelaide, South Australia, Australia.
[b] Division of Materials Science, Faculty of Advanced Science and Technology Kumamoto University, Kumamoto 860-8555, Japan
*Email: dusan.losic@adelaide.edu.au

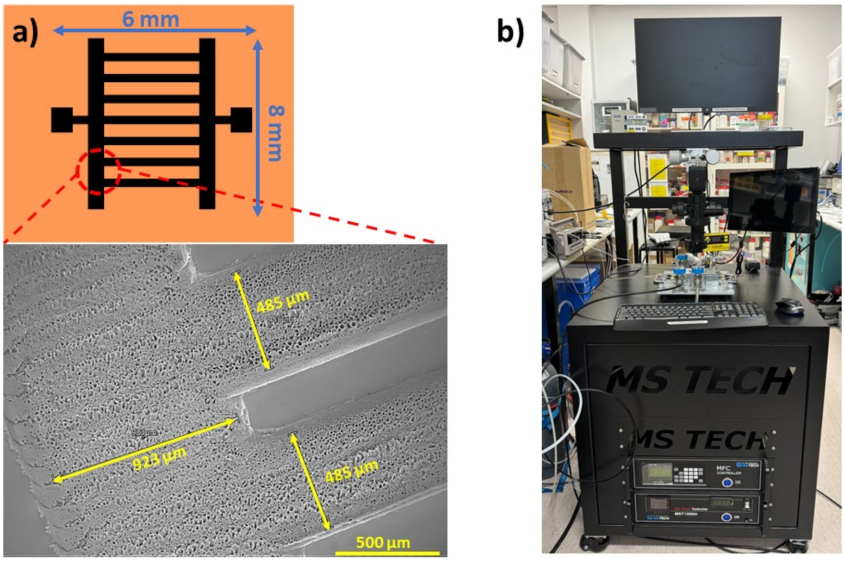

Figure S1. a) Modified IDE electrode design for LSG fabrication. b) Realistic images of gas sensing systems used

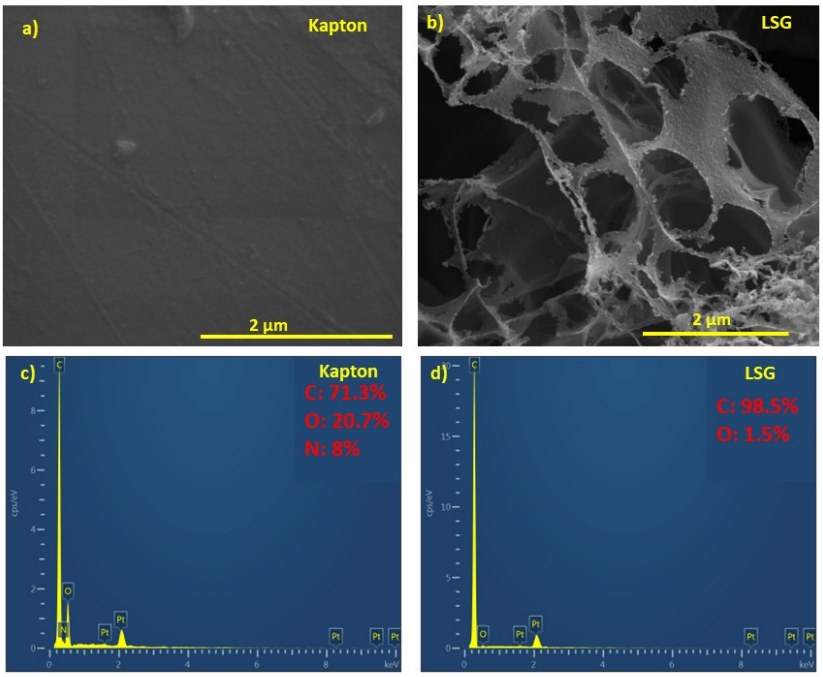

Figure S2. a,b) SEM images of Kapton and LSG; c,d) EDX of Kapton and LSG

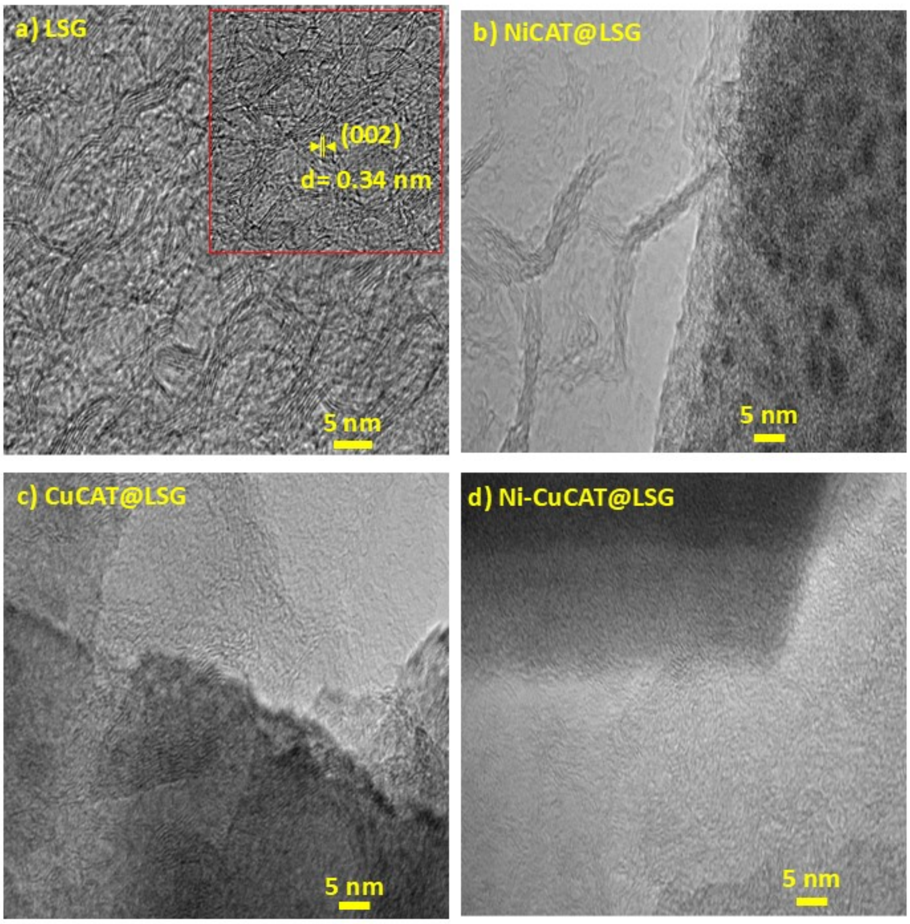

Figure S3. HR-TEM images of a) LSG, b) NiCAT@LSG, c) CuCAT@LSG and d) Ni-CuCAT@LSG

Table T1. EDS and XPS summary table of conductive MOFs and MOFs grown on LSG

EDX	**Atomic % (Average 5 points)**			
	C	**O**	**Ni**	**Cu**
LSG	98.5	1.5	-	-
NiCAT@LSG	88.2	9.46	2.34	-
CuCAT@LSG	81.16	14.88	-	3.96
Ni-CuCAT@LSG	88.175	8.725	1	2.1
NiCAT	76.24	18.12	5.64	-
CuCAT	73.48	20.36	-	6.16
Ni-CuCAT	75.84	17.12	2.18	4.86
XPS	**Atomic %**			
LSG	88.05	11.95	-	-
NiCAT@LSG	75.99	22.79	1.22	-
CuCAT@LSG	92.21	7.57	-	0.22
Ni-CuCAT@LSG	77.65	21.22	0.32	0.81
NiCAT	74.96	23.95	1.09	-
CuCAT	77.70	20.80	-	1.50
Ni-CuCAT	76.71	22.02	0.42	0.84

Table T2. Summary of lattice parameters of materials from XRD and TEM

	d_{XRD} (nm)			d_{TEM} (nm)
	(100)	(001)	(002)	
LSG	-	-	**0.338**	0.34±0.01
NiCAT@LSG	**1.889**	0.328	-	1.94±0.05 for NiCAT and 0.34±0.01 for LSG
CuCAT@LSG	**1.814**	0.320	-	1.84±0.05 for CuCAT and 0.34±0.01 for LSG
Ni-CuCAT@LSG	**1.809**	0.318	-	1.81±0.05 for Ni-CuCAT and 0.34±0.01 for LSG
NiCAT	**1.967**	0.330	-	1.95±0.05
CuCAT	**1.843**	0.323	-	1.83±0.05
Ni-CuCAT	**1.821**	0.319	-	1.80±0.05

Description: The d spacing from XRD is calculated by using peak position (2θ), order of reflection (n) and x-ray wavelength (λ). Based on Bragg's Law, the interplanar spacing (d) is calculated using this equation:

Interplanar spacing (d) = Order of Reflection (n) × Wavelength (λ) / 2 × Sinθ with λ= 0.15418 and n=1

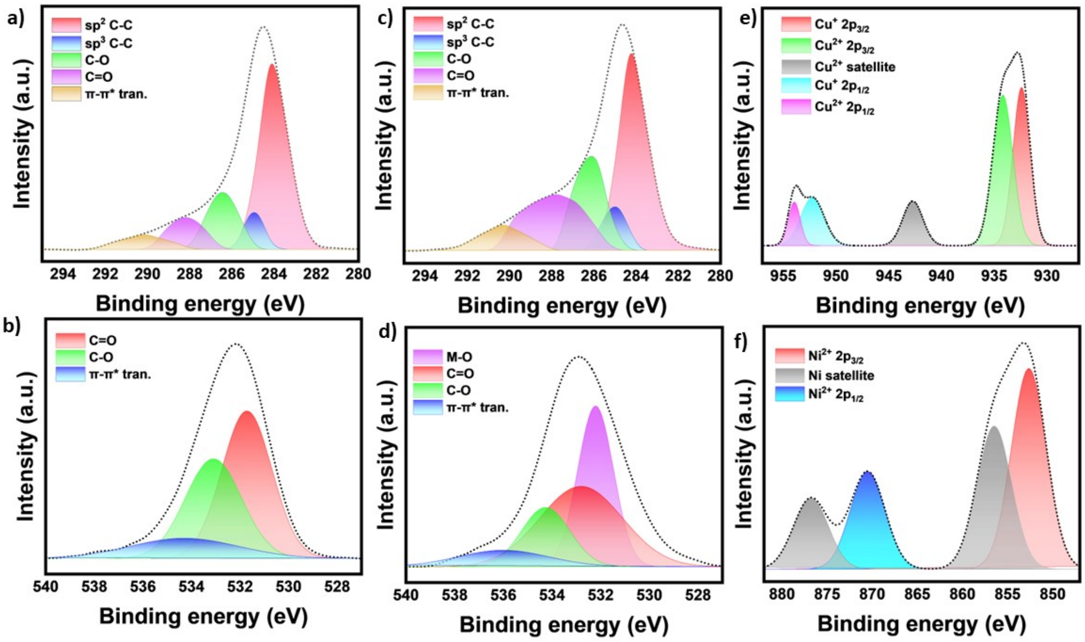

Figure S4. Chemical composition analysis by XPS. a, b) XPS C 1s and O 1s spectra of LSG, respectively. c, d, e, f) XPS C 1s, O 1s, Cu 2p and Ni 2p of Ni-CuCAT@LSG, respectively

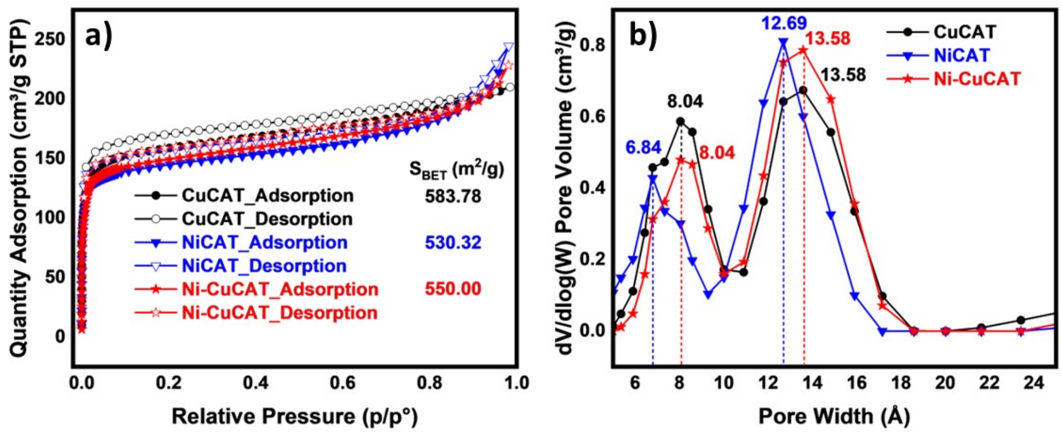

Figure S5. a) Surface area and b) pore size distribution of M-CAT measured by BET analysing

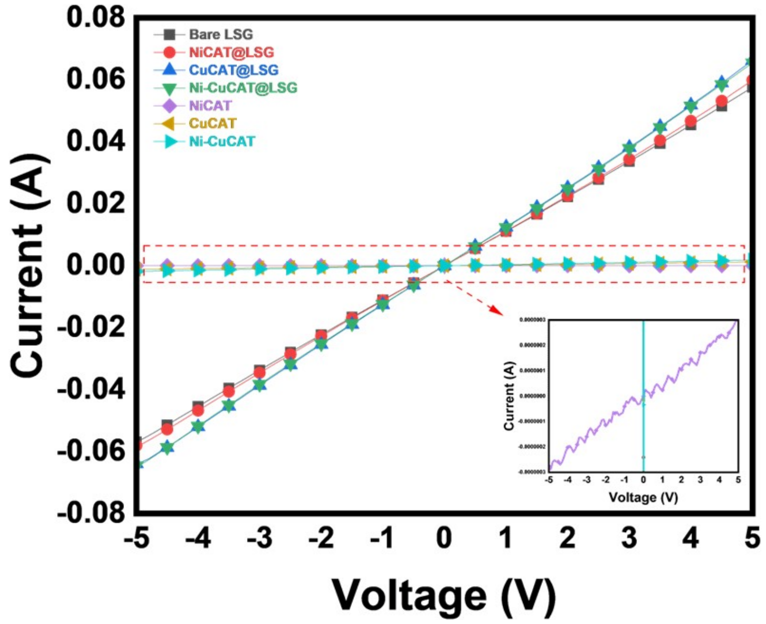

Figure S6 Current-voltage (I-V) curve of bare LSG, NiCAT@LSG, CuCAT@LSG, Ni-CuCAT@LSG, NiCAT, CuCAT and Ni-CuCAT.

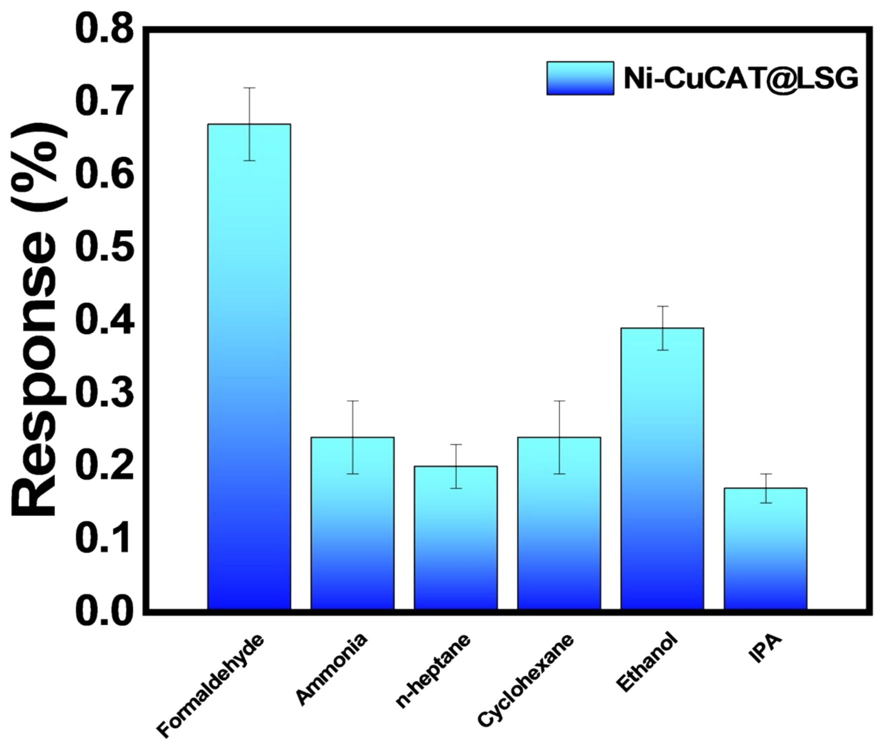

Figure S7 a) Selectivity study of Ni-CuCAT@LSG sensor for different VOCs.

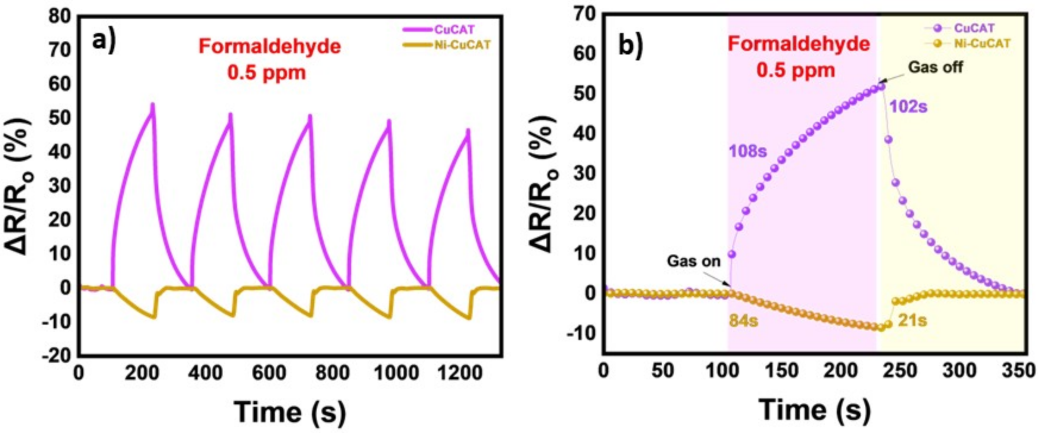

Figure S8 Real time response at room temperature of fabricated sensors for 0.5 ppm formaldehyde. a) Response and recovery curve of CuCAT and Ni-CuCAT. b) Response time and recovery time of CuCAT and NiCuCAT

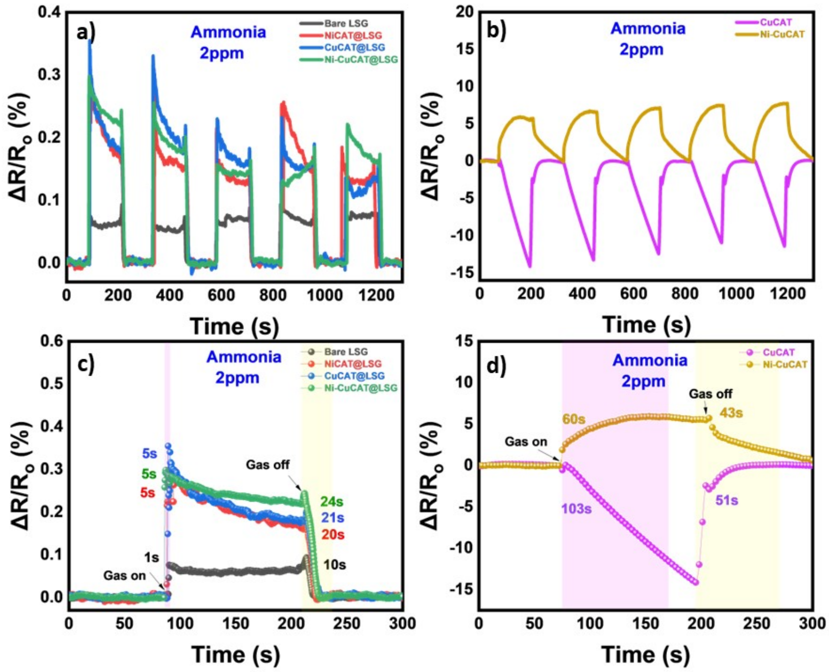

Figure S9 Real time response at room temperature of fabricated sensors for 2 ppm ammomia. a) Response and recovery curve of Ni-CuCAT@LSG, CuCAT@LSG, NiCAT@LSG and bare LSG. b) Response and recovery curve of CuCAT and Ni-CuCAT. c) Response time and recovery time of of Ni-CuCAT@LSG, CuCAT@LSG, NiCAT@LSG and bare LSG. d) Response time and recovery time of CuCAT and NiCuCAT

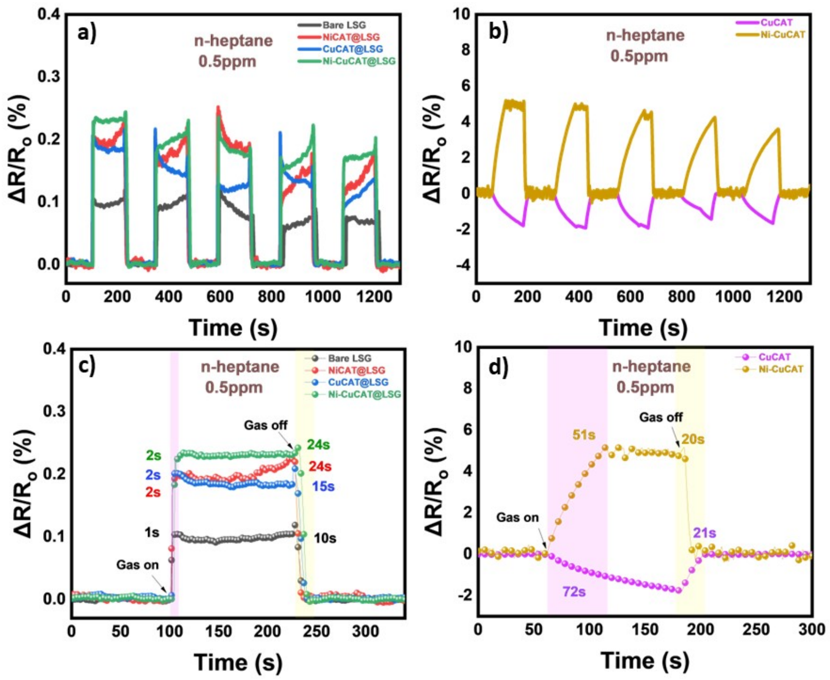

Figure S10 Real time response at room temperature of fabricated sensors for 0.5 ppm n-heptane. a) Response and recovery curve of Ni-CuCAT@LSG, CuCAT@LSG, NiCAT@LSG and bare LSG. b) Response and recovery curve of CuCAT and Ni-CuCAT. c) Response time and recovery time of of Ni-CuCAT@LSG, CuCAT@LSG, NiCAT@LSG and bare LSG. d) Response time and recovery time of CuCAT and NiCuCAT.

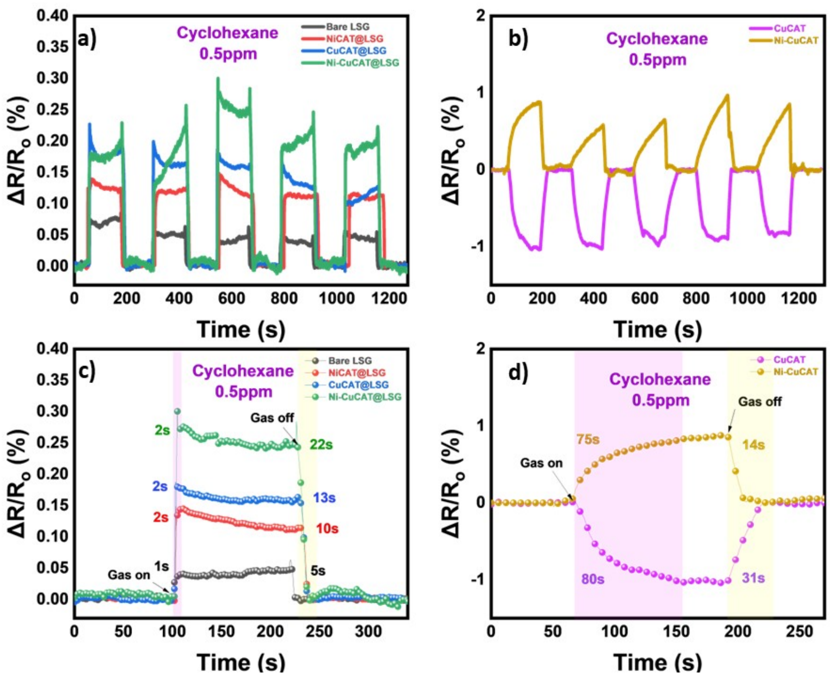

Figure S11 Real time response at room temperature of fabricated sensors for 0.5 ppm cyclohexane. a) Response and recovery curve of Ni-CuCAT@LSG, CuCAT@LSG, NiCAT@LSG and bare LSG. b) Response and recovery curve of CuCAT and Ni-CuCAT. c) Response time and recovery time of of Ni-CuCAT@LSG, CuCAT@LSG, NiCAT@LSG and bare LSG. d) Response time and recovery time of CuCAT and NiCuCAT.

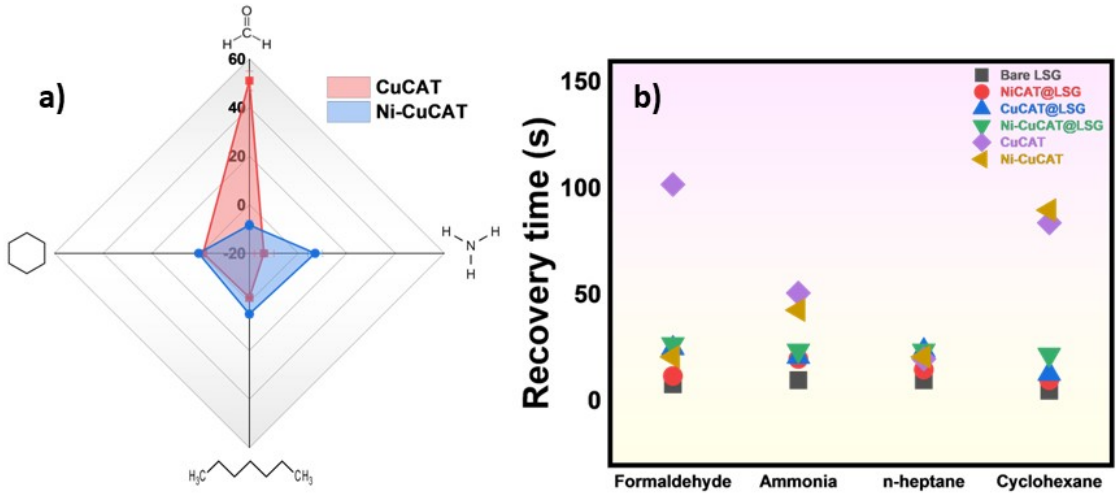

Figure S12 a) Selectivity study of MOFs based sensor devices for different VOCs. b) Comparative recovery time of MOFs@LSG based sensor devices for different VOCs.

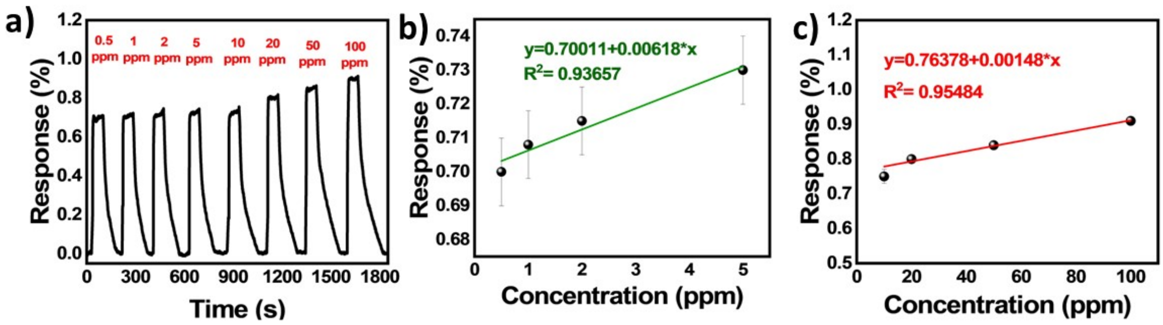

Figure S13 a) Response curves of Ni-CuCAT@LSG with different concentrations (0.5 – 100 ppm) of formaldehyde. b) Linear relationship between concentration and sensitivity in low concentration range from 0.5 to 5 ppm formaldehyde of Ni-CuCAT@LSG sensor. c) Linear relationship between concentration and sensitivity in high concentration range from 10 to 50 ppm formaldehyde of Ni-CuCAT@LSG

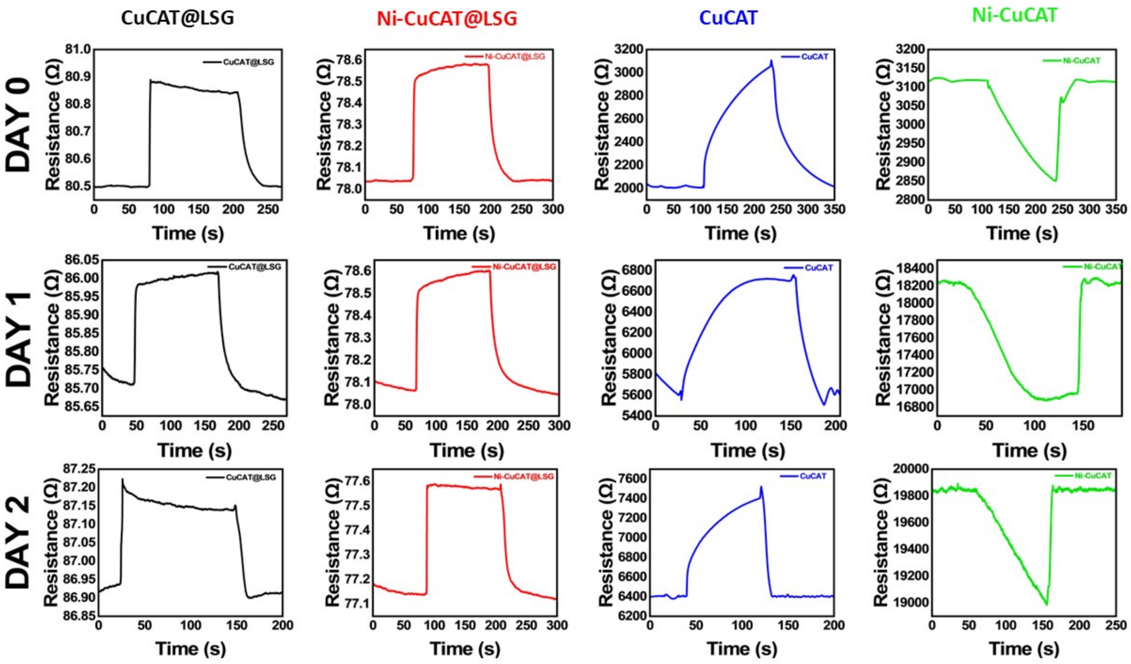

*Figure S14 Resistance response with 0.5 ppm formaldehyde at RT of CuCAT@LSG (black), Ni-CuCAT@LSG (red), CuCAT (blue) and Ni-CuCAT (green) from **day 0 to day 1***

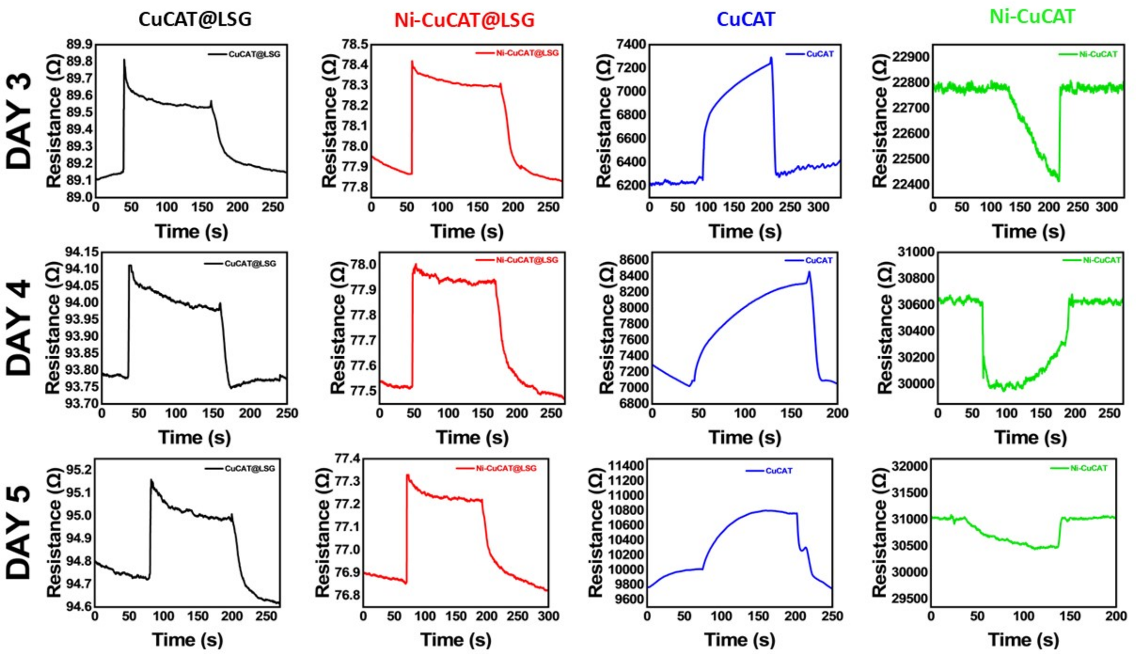

*Figure S15 Resistance response with 0.5 ppm formaldehyde at RT of CuCAT@LSG (black), Ni-CuCAT@LSG (red), CuCAT (blue) and Ni-CuCAT (green) from **day 3 to day 5***

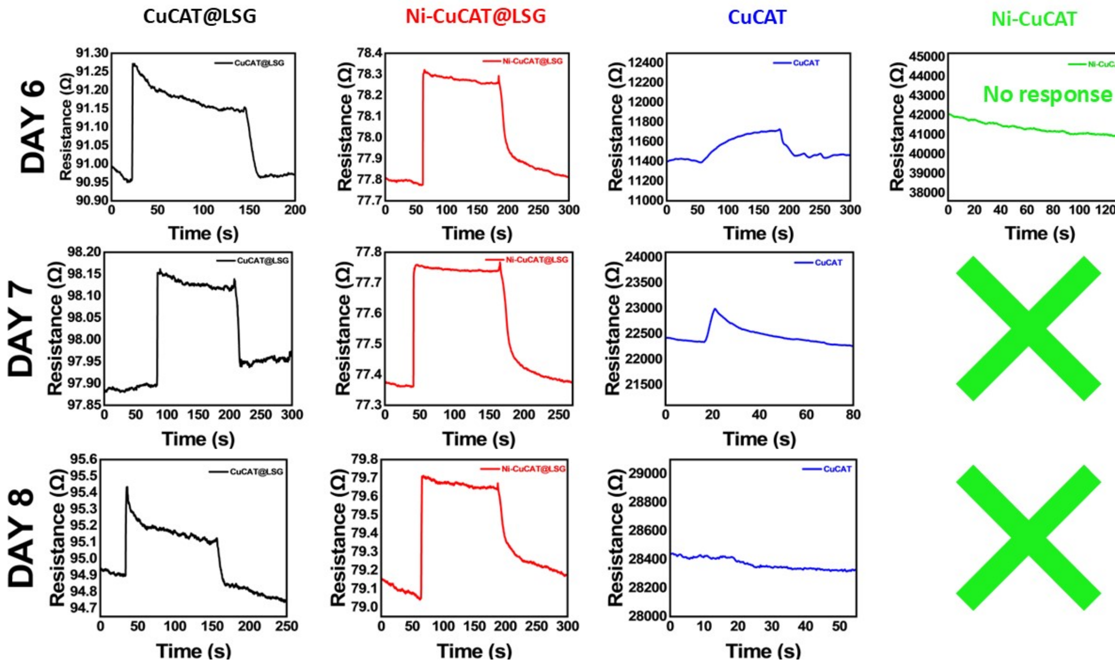

*Figure S16 Resistance response with 0.5 ppm formaldehyde at RT of CuCAT@LSG (black), Ni-CuCAT@LSG (red), CuCAT (blue) and Ni-CuCAT (green) from **day 6 to day 8***

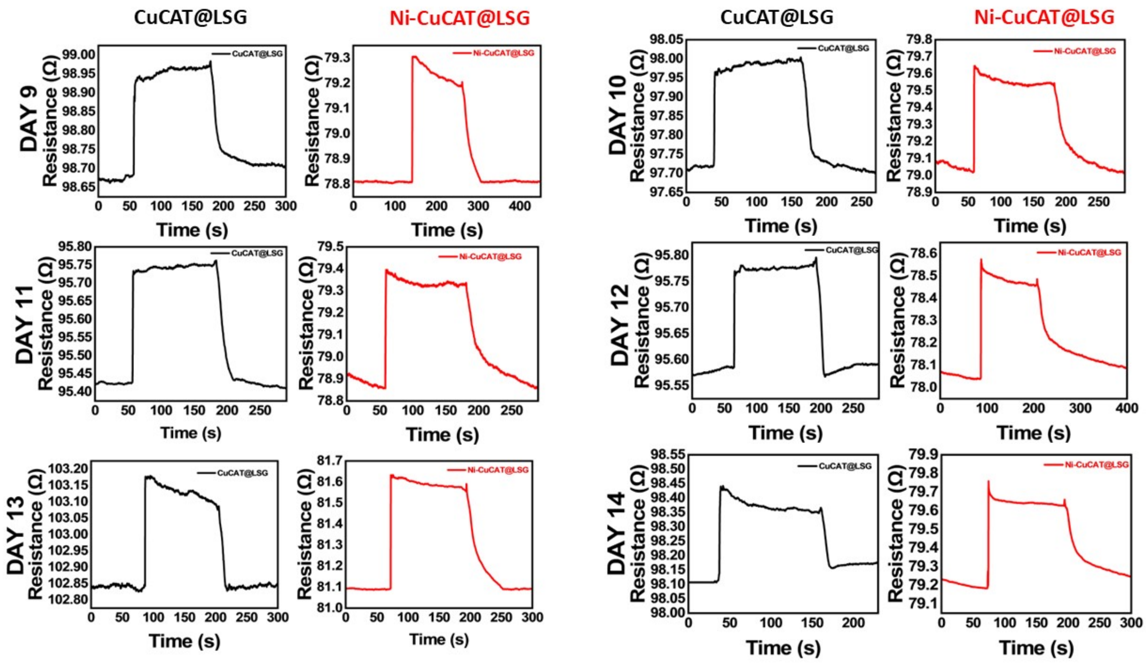

*Figure S17 Resistance response with 0.5 ppm formaldehyde at RT of CuCAT@LSG (black) and Ni-CuCAT@LSG (red) from **day 9 to day 14***

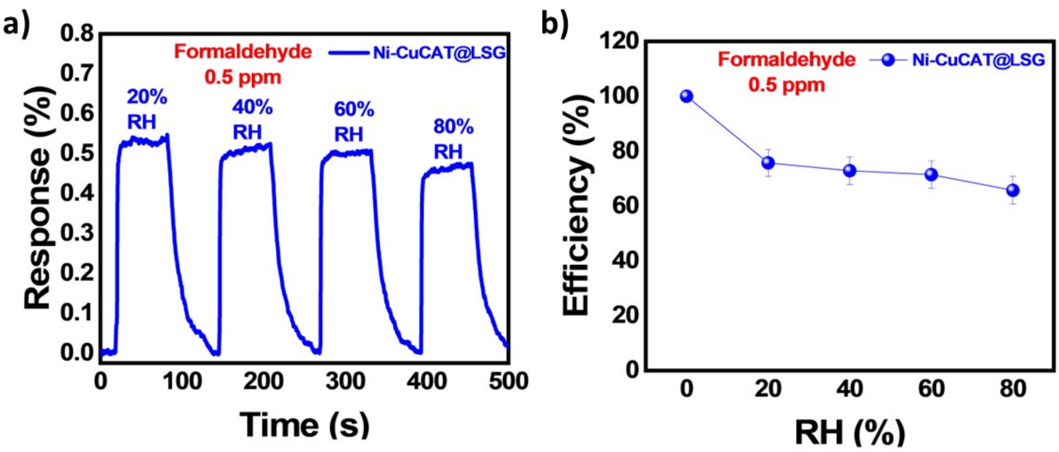

Figure S18 a) Response curves of Ni-CuCAT@LSG with 0.5 ppm formaldehyde at different relative humidity condition, b) Efficiency of Ni-CuCAT@LSG at different humidity environment when exposure to 0.5 ppm formaldehyde

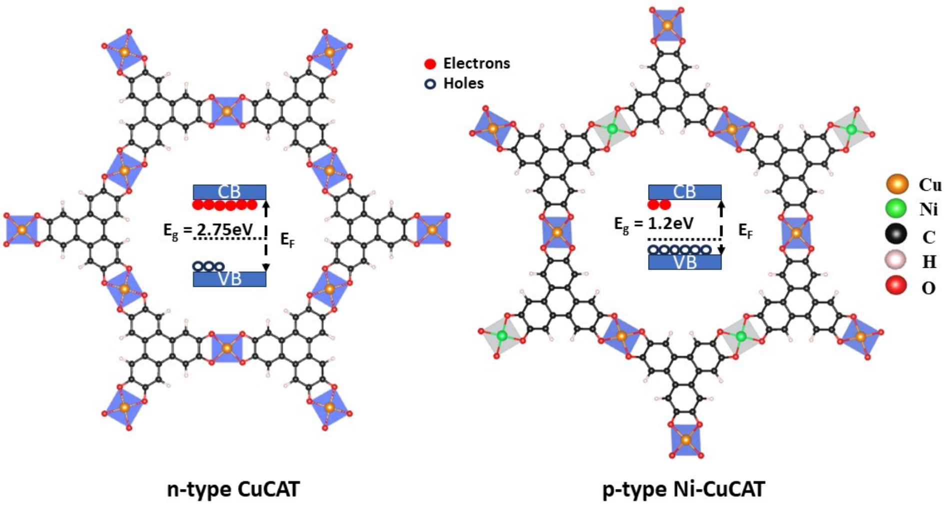

Figure S19 Schematic illustrations of energy band diagrams of CuCAT and Ni-CuCAT

Table T3 Signal to noise ratios (SNRs) of sensors when exposed to target gas (0.5 ppm) at RT.

Target Gas	Signal to noise ratio (SNR)			
	LSG	Ni-CuCAT@LSG	CuCAT@LSG	NiCAT@LSG
Formaldehyde	19.61	170.73	71.30	27.83
Ammonia	9.82	32.78	64.17	30.21
n-heptane	12.64	30.21	27.13	29.03
Cyclohexane	7.84	31.54	29.42	25.12

Table T4 Comparison table with other state-of-the-art formaldehyde sensing materials.

Materials	HCHO concentration (ppm)	Response (%)	Response/ Recovery time (s)	Temp (°C)	Ref.	Published Year
5MMM ZIF-7/TiO_2	5	[a]11000	9/400	RT	[1]	2021
β-Ga_2O_3	300	[a]30.25	870/1055	300	[2]	2024
ZnO nanorod	400	[b]12000	10/-	100	[3]	2023
In_2O_3@TiO_2	1	[c]5.3	24/52	RT	[4]	2024
CuO/In_2O_3	10	[c]11.67	77/110	100	[5]	2022
MXene/NiO-P2	2	[c]0.8	279/346	RT	[6]	2023
Pt_1-In_2O_3	100	[c]750.4	2/373	200	[7]	2024
In_2O_3 nanospheres	100	[c]20	142/135	180	[8]	2022
Cr_2O_3/$ZnSnO_3$	50	[c]37.8	4/4	175	[9]	2024
$NiCo_2O_4$ nanoneedles	50	[a]1.85	22/57	RT	[10]	2023
Mn-NiO	100	[c]12593	5/5	RT	[11]	2022
NiS/Ni-ZnO	10	[d]330	39.4/40.7	RT	[12]	2022
ZnO/ANS/rGO	5	[c]1.05	300/-	RT	[13]	2021
$ZnSnO_3$/MXene	5	[a]62.4	6.2/5.1	RT	[14]	2022
SnO2/MXene	50	[a]1.01	36/44	RT	[15]	2021
rGO/ZnO NRs	1	[a]21	82/167	RT	[16]	2017
rGO/ZnO	10	[a]5.2	117/-	RT	[17]	2015
$Ti_3C_2T_x$/SnO_2	10	[a]29.16	388/486	RT	[18]	2023
ZIF-8@LSG	0.8	[a] 0.045	3/22	RT	[19]	2024
Ni-CuCAT	0.5	[a]8.4	84/21	RT	This work	-
CuCAT	0.5	[a]51	108/102	RT	This work	-
Ni-CuCAT@LSG	0.5	[a]0.42	2/25	RT	This work	-
Ni-CuCAT@LSG	**0.5**	**[a]0.7**	**2/27**	**RT**	**This work**	**-**

RT-Room temperature. [a] Response (%)= $|\Delta R/R_o|$. [b] Response = $|\Delta I/I_o|$. [c] Response = R_a/R_g. [d] Response = I_g/I_a.

Reference

(1) Jo, Y. K.; Jeong, S. Y.; Moon, Y. K.; Jo, Y. M.; Yoon, J. W.; Lee, J. H. Exclusive and ultrasensitive detection of formaldehyde at room temperature using a flexible and monolithic chemiresistive sensor. *Nat Commun* **2021,** *12* (1), 4955, DOI: 10.1038/s41467-021-25290-3.

(2) Giri, S.; Mahata, B.; Guha, P. K.; Banerji, P. β-Ga2O3 Nanostructure-Based Chemiresistive Sensor for Selective Detection of Formaldehyde. *ACS Applied Electronic Materials* **2024,** *6* (1), 230-241, DOI: 10.1021/acsaelm.3c01187.

(3) Sinha, M.; Neogi, S.; Ghosh, R. Temperature dependent selectivity switching from methanol to formaldehyde using ZnO nanorod based chemi-resistive sensor. *Sensors and Actuators A: Physical* **2023,** *357*, DOI: 10.1016/j.sna.2023.114405.

(4) Zhang, S.; Li, Y.; Wu, T.; Zhao, Z.; Feng, Q.; Li, X. Nanocube-shaped In2O3@TiO2 core-shell based chemiresistive-type sensors for formaldehyde detection at room temperature. *Sensors Actuators B: Chem.* **2024,** *408*, DOI: 10.1016/j.snb.2024.135540.

(5) Dan, M.; Qiao, T.; Wang, G.; Shen, Y.; San, X.; Li, R.; Meng, F. Rational design of CuO/In2O3 heterostructures with flower-like structures for low temperature detection of formaldehyde. *J. Alloys Compd.* **2022,** *896*, DOI: 10.1016/j.jallcom.2021.162959.

(6) Huang, B.; Tong, X.; Zhang, X.; Feng, Q.; Rumyantseva, M. N.; Prakash, J.; Li, X. MXene/NiO Composites for Chemiresistive-Type Room Temperature Formaldehyde Sensor. *Chemosensors* **2023,** *11* (4), DOI: 10.3390/chemosensors11040258.

(7) Bu, W.; Liu, N.; Zhang, Y.; Han, W.; Chuai, X.; Zhou, Z.; Hu, C.; Lu, G. Atomically dispersed Pt on MOF-derived In2O3 for chemiresistive formaldehyde gas sensing. *Sensors Actuators B: Chem.* **2024,** *404*, DOI: 10.1016/j.snb.2023.135260.

(8) Cao, J.; Zhang, N.; Yang, S.; Xu, W.; Zhang, X.; Zhang, H.; Wang, S. Study on the selectivity difference of formaldehyde and ethanol induced by variation of energy gap in In2O3 hierarchical materials. *Colloids Surf. Physicochem. Eng. Aspects* **2022,** *648*, DOI: 10.1016/j.colsurfa.2022.129306.

(9) Jiang, L.; Zhang, R.; Zhang, W.; Yang, J.; Jiang, H.; Hu, Z.; Zhang, Y. High response to formaldehyde gas and ppb-level detectability of nanoparticle Cr2O3/ porous cubic ZnSnO3 composites p-n heterojunction gas sensor. *Ceram. Int.* **2024,** *50* (4), 6950-6960, DOI: 10.1016/j.ceramint.2023.12.045.

(10) Karmakar, S.; Sett, A.; Chandra Maity, P.; Sha, R.; Kanti Bhattacharyya, T.; Lahiri, I. A highly selective room-temperature formaldehyde gas sensor based on vertically aligned 1D NiCo2O4 nanoneedles. *Mater. Lett.* **2023,** *350*, DOI: 10.1016/j.matlet.2023.134927.

(11) John, R. A. B.; Shruthi, J.; Ramana Reddy, M. V.; Ruban Kumar, A. Manganese doped nickel oxide as room temperature gas sensor for formaldehyde detection. *Ceram. Int.* **2022,** *48* (12), 17654-17667, DOI: 10.1016/j.ceramint.2022.03.036.

(12) Yang, Y.; Wu, S.; Cao, Y.; Li, S.; Xie, T.; Lin, Y.; Li, Z. A highly efficient room-temperature formaldehyde gas sensor based on a Ni-doped ZnO hierarchical porous structure decorated with NiS illuminated by UV light. *J. Alloys Compd.* **2022,** *920*, DOI: 10.1016/j.jallcom.2022.165850.

(13) Fan, J.; Li, H.; Hu, H.; Niu, Y.; Hao, R.; Umar, A.; Al-Assiri, M. S.; Alsaiari, M. A.; Wang, Y. An insight into improvement of room temperature formaldehyde sensitivity for graphene-based gas sensors. *Microchem. J.* **2021,** *160*, DOI: 10.1016/j.microc.2020.105607.

(14) Sima, Z.; Song, P.; Ding, Y.; Lu, Z.; Wang, Q. ZnSnO3 nanocubes/Ti3C2Tx MXene composites for enhanced formaldehyde gas sensing properties at room temperature. *Appl. Surf. Sci.* **2022,** *598*, DOI: 10.1016/j.apsusc.2022.153861.

(15) He, T.; Liu, W.; Lv, T.; Ma, M.; Liu, Z.; Vasiliev, A.; Li, X. MXene/SnO2 heterojunction based chemical gas sensors. *Sensors Actuators B: Chem.* **2021,** *329*, DOI: 10.1016/j.snb.2020.129275.

(16) Minh Triet, N.; Thai Duy, L.; Hwang, B. U.; Hanif, A.; Siddiqui, S.; Park, K. H.; Cho, C. Y.; Lee, N. E. High-Performance Schottky Diode Gas Sensor Based on the Heterojunction of Three-Dimensional Nanohybrids of Reduced Graphene Oxide-Vertical ZnO Nanorods on an AlGaN/GaN Layer. *ACS Appl Mater Interfaces* **2017,** *9* (36), 30722-30732, DOI: 10.1021/acsami.7b06461.

(17) Li, X.; Wang, J.; Xie, D.; Xu, J.; Dai, R.; Xiang, L.; Zhu, H.; Jiang, Y. Reduced graphene oxide/hierarchical flower-like zinc oxide hybrid films for room temperature formaldehyde detection. *Sensors Actuators B: Chem.* **2015,** *221*, 1290-1298, DOI: 10.1016/j.snb.2015.07.102.
(18) Zhang, Y.; Wang, M.-Y.; San, X.-G.; Shen, Y.-B.; Wang, G.-S.; Zhang, L.; Meng, D. Ti3C2Tx/SnO2 P–N heterostructure construction boosts room-temperature detecting formaldehyde. *Rare Metals* **2023,** *43* (1), 267-279, DOI: 10.1007/s12598-023-02456-0.
(19) Tran, A. T. T.; Hassan, K.; Tung, T. T.; Tripathy, A.; Mondal, A.; Losic, D. Graphene and metal-organic framework hybrids for high-performance sensors for lung cancer biomarker detection supported by machine learning augmentation. *Nanoscale* **2024,** *16* (18), 9084-9095, DOI: 10.1039/d4nr00174e.